Principles of a Three-Axis Vibrating Gyroscope

B. J. GALLACHER

J. S. BURDESS

A. J. HARRIS
University of Newcastle
UK

M. E. McNIE
DERA
UK

The principal features of a three-axis ring gyroscope are described. The equations of motion, the response to constant rates of turn, and the relationships between the modes of vibration are derived. Tuned and untuned cases are considered.

Manuscript received July 14, 2000; revised June 28, 2001; released for publication August 3, 2001.

IEEE Log No. T-AES/37/4/10997.

Refereeing of this contribution was handled by J. L. Leva.

This work was supported by EPSRC under GR/M13756 and Technology Group 07 of UK MoD as part of its Corporate Research Programme.

Authors' addresses: B. J. Gallacher and J.S. Burdess, Dept. of MMM Engineering, University of Newcastle, Newcastle upon Tyne, UK, NE1 7RU, E-mail: (b.j.gallacher@ncl.ac.uk); A. J. Harris, Dept. of Electrical Engineering, University of Newcastle, Newcastle upon Tyne, UK, NE1 7RU; M. E. McNie, DERA (Malvern), St. Andrews Road, Malvern, Worcs, UK, WR14 3PS.

I. NOMENCLATURE

ω_i	Natural angular frequency $i = 1,2,3,4$
Ω	Applied rate of turn
X, Y, Z	Fixed set of input axes
x, y, z	Set of local axes
a	Ring radius
b	Ring width
d	Ring depth
h	Ligament width
L_1, L_2, L_3	Ligament beam length
u	Radial displacement in x direction
v	Tangential displacement in y direction
w	Vertical displacement in z direction
T	Ring kinetic energy
D	Rayleigh dissipation function
c	Viscous friction parameter
V_r	Strain energy of ring
V_l	Potential energy of ring support ligaments
q_i	Generalized coordinates $i = 1,2,3,4$
$\mathbf{q}$	Vector of Generalized coordinates $\mathbf{q} = (q_1, q_2, q_3, q_4)^{\mathrm{T}}$
β	Parasitic twisting angle
β_i	Generalized coordinates of twisting angle $i = 3,4$
k_i	Generalized stiffness coefficients of ring $i = 1,2,3,4$
k_n, k_{ij}	Generalized stiffness coefficients of ligaments
m_i	Generalized mass of ring $i = 1,2,3,4$
$I_{xx}, I_{zz}, I'_{zz}, I'_{yy}$	Second moment of area of ring section
$I_{\theta\theta}, I'_{\theta\theta}$	Torsional section factors
E	Modulus of elasticity
G	Modulus of rigidity
ν	Poisson's ratio
A	Cross sectional area of ring
ρ	Density
ξ_i	Damping ratio $i = 1,2,3,4$
B	Bandwidth
$\lambda, \lambda', \lambda''$	Gyroscopic coupling factors
n, m	Mode order
φ	Phase
ϕ	Gradient of centre line of ring
η	Miss tuning factor
q_{0i}	Amplitude $i = 1,2,3,4$
κ_1, κ_2, τ	Components of curvature and twist
W, R, Q	Forces applied to ligament
M, M_g, M_d	Moments applied to ligament
M_r, M_s, M_t	Bending moments in ligament due to in-plane motion
M_x, M_y	Bending moments in ligament due to out-of-plane motion
μ	Ratio of q_i/β_i, $i = 1,2,3,4$.

II. INTRODUCTION

Gyroscopes are used in various applications to either measure the rate of rotation about a defined axis or measure the angle turned. Traditional gimballed gyroscopes use the inertial properties of a spinning wheel and can only measure rate of rotation about one axis. Two or three of these must be employed if rotations about two or three orthogonal axes are to be sensed. Vibrating gyroscopes are another class of gyro, which offer important advantages over the gimballed design. They offer the possibility of sensing rotation about more than one axis, are generally smaller, require less power and the bearings and drive motor required in the gimballed design are removed in the vibrating gyro. With one exception the vibrating gyroscope has not been developed to inertial performance and its use has been limited to rate of turn applications.

Forms of vibrating gyroscopes include BAe's Vibrating Structure Gyroscope (VSG) [1] which uses a piezo-ceramic cylinder as the sensing element and Delco's Hemispherical Resonator Gyroscope (HRG) [15], which uses a fused silica hemispherical shell as the sensing element and is electrostatically actuated and sensed. In both of these single axis devices the modes of vibrations used to detect the rate of turn via Coriolis coupling share the same natural frequency thus enabling amplitude multiplication to improve sensitivity. The HRG has achieved inertial navigation performance.

The recent development of MEMS technology has enabled the size of the vibrating gyroscope to be very much reduced and a number of designs have been manufactured by this technology. Typical examples include the single axis Micromachined Angular Rate Sensor (MARS-RR) manufactured by HSG-IMIT [14], the vibrating nickel ring gyroscope of General Motors (again a single axis device) [11], and the silicon ring gyroscope of British Aerospace [16]. The first two of these examples use capacitive methods for actuation and sensing while the third uses electromagnetic methods. Other similar designs are referenced in [17] and it is shown that tuning of the modes of the gyroscope, to improve sensitivity, has so far been limited to "ring type" designs. Juneau, et al. [18], has shown that two-axis designs are possible.

In this work it is shown that the ring form of gyroscope is capable of being further developed to a rate sensor that can measure rates of turn about three orthogonal axes. The equations of motion of the device are derived using a Lagrangian method and the response to applied rate is calculated. It is shown how maximum sensitivity can be achieved by tuning those natural frequencies of the ring associated with rate measurement. The issues associated with the tuning of the natural frequencies of the ring are discussed.

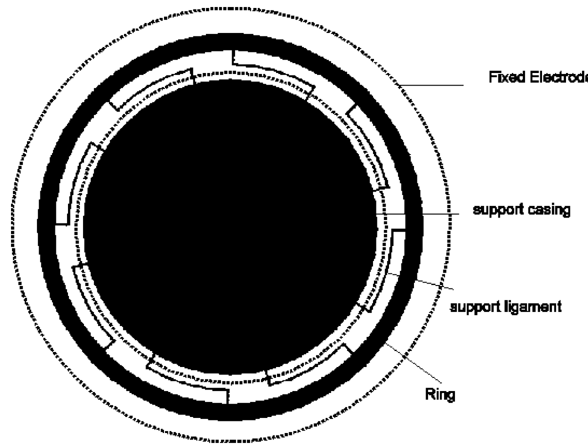

Fig. 1. Basic form of gyroscope.

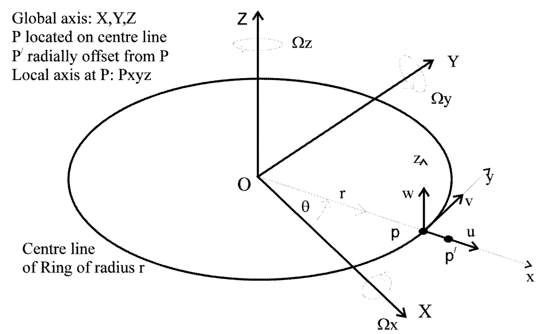

Fig. 2. Coordinate system.

III. INPUT AND OUTPUT AXES OF RING GYROSCOPE AND GENERAL DESCRIPTION OF BEHAVIOR

The planar structure shown in Fig. 1 illustrates the basic form of the gyroscope discussed here. The principal features of the design are the axi-symmetry of the ring sensing element and the cyclic-symmetric arrangement of the ligaments which connect the ring to the supporting casing. These features allow important modes of vibration of the structure to exist in degenerate pairs [6], and this enables the sensitivity to applied rate of turn to be improved by matching the natural frequencies of those modal responses associated with rate measurement [3]. If this matching is not preserved three axis measurements are still possible but the sensitivity of the sensing element to applied rates of turn is much reduced.

Fig. 2 illustrates the center line of the ring. Reference axes OXYZ are fixed to the supporting casing and it is assumed that OZ is perpendicular to the plane containing the structure, with O at the center of the ring. It is assumed that these axes rotate with an angular velocity $\mathbf{\Omega} = (\Omega_x, \Omega_y, \Omega_z)$. Motion of the ring relative to OXYZ is represented by the displacement $\mathbf{r}$ of a typical point P on its center line. This displacement is measured with respect to the local polar coordinate axes at P and is expressed

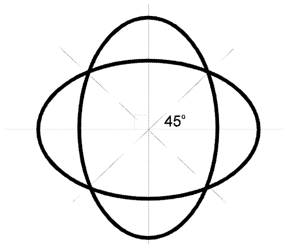

Fig. 3. $\cos 2\theta$ modal displacement.

by $\mathbf{r} = (u, v, w)^T$, where u, v, and w are the radial, tangential, and axial components, respectively.

When operated as a gyroscope a natural in-plane mode of the ring will be driven at a set amplitude of vibration at its natural frequency ω_1. This motion, which is referred to as the primary mode of the gyroscope, is characterized by radial u, and tangential v, displacements having spatial variations of the form $\cos n\theta$ and $\sin n\theta$, respectively, where n is the mode number. Fig. 3 shows the extreme modal displacement corresponding to the radial motion for the case $n = 2$. When a rate of turn Ω_z is applied about the input axis OZ Coriolis inertial forces are generated and these will excite a secondary motion, which also lies in the plane of the ring. In general this secondary response is characterized by a mode with natural frequency ω_2 and has a spatial form given by $u \sim \sin n\theta$ and $v \sim \cos n\theta$. For the ideal cyclic form shown in Fig. 1 these modes form a degenerate pair and $\omega_1 = \omega_2$. In this case this primary and secondary motions are said to be tuned. Measuring the amplitude of this secondary mode or the actuation needed to null it will provide a measure of Ω_z.

In a similar fashion a rate of turn Ω_x applied about the casing axis OX will again give rise to Coriolis inertia forces. These inertia forces, however, act in a direction perpendicular to the plane of the ring (along OZ) and thus excite a secondary response in the ring in that direction. It is shown in what follows that this out-of-plane secondary response is related to a mode shape of the ring that has a spatial variation along OZ of the form $\sin(n \pm 1)\theta$ with a corresponding natural frequency ω_3. The measurement of this motion or the actuation needed to null it will provide a measurement of Ω_x. Likewise a rate of turn Ω_y about the axis OY will produce a similar out of plane response but with a related mode shape of $\cos(n \pm 1)\theta$ and a corresponding natural frequency ω_4. Fig. 4 shows this mode shape for the case $n + 1 = 3$. However, as a result of the cyclic form imposed on the structure it follows that these out-of-plane modes are degenerate and that $\omega_3 = \omega_4$ for the ideal form. Although the natural frequencies of the out of plane modes are tuned to each other the cyclic form of the structure does not guarantee their tuning with the frequency of the in-plane primary motion. Such tuning can only be achieved by making the out-of-plane thickness

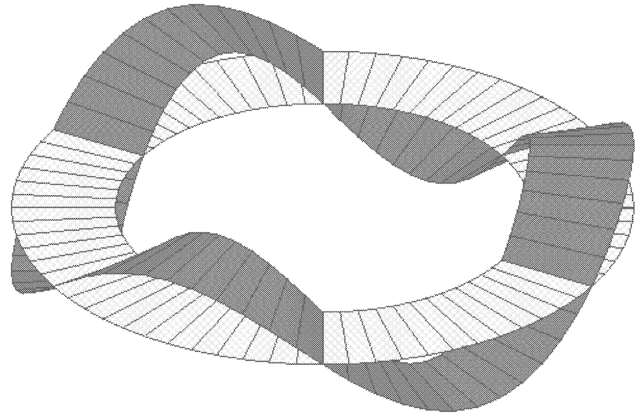

Fig. 4. $\cos 3\theta$ modal displacement.

of the structure have an appropriate value or by modifying the out-of-plane stiffness of the structure electrostatically using the approach described in [3].

In the dynamic analysis of the gyro structure it is assumed that the ring is the significant inertial element and that the contribution made by the mass of the supporting ligaments can be neglected. This assumption has the advantage of greatly simplifying the analysis and allows the principal dynamic features of the gyroscope to be identified and discussed in simple terms. Elasticity of the ligaments is considered and their effect on the natural frequencies and thus tuning is determined.

IV. DESCRIPTION OF IDEAL RING

The ring used to model the gyroscope has a rectangular cross section, width b and depth d, and in the unstressed state its centre line forms a circle of radius a. Excluding rigid body motion, the modes of vibration of such a ring are known, [5, 9], to be determined by extensional, torsional, and flexural motions. Purely extensional and torsional modes occur only at high frequencies and are, respectively, the result of circumferential strain in the center line and the rotation of adjacent sections about the centre line. The modes of principal interest in the case of the gyroscope are the low frequency modes associated with the flexural motion of the ring and these occur when the center line is either bent in the plane of the ring or bent out of the plane of the ring without circumferential strain. At this point it needs to be appreciated that although the out-of-plane flexural mode is predominantly one of pure translation of the ring section along OZ it is accompanied by a parasitic rotation of the section about the center line. A detailed description of this coupled behavior is presented in [5, 9].

The flexural modes of the ring relevant to the motion of the gyroscope can be used to define the radial, tangential, and axial displacements of a point on the center line of the ring and these can be shown to be of the form

$$u = q_1 \cos n\theta + q_2 \sin n\theta \tag{1}$$

$$v = -\frac{1}{n}(q_1 \sin n\theta - q_2 \cos n\theta) \tag{2}$$

$$w = q_3 \cos m\theta + q_4 \sin m\theta \tag{3}$$

where $m = n \pm 1$ and q_i are generalized coordinates which represent the contribution made by each mode to the motion. These displaced shapes are those corresponding to the mode shapes of an unsupported ring [5] and it is assumed that the presence of ligaments does not significantly modify the shape of the motion. To derive the equations of motion of the gyroscope based upon the mode shapes defined by (1), (2), and (3) a Lagrangian approach is used and this requires the kinetic and strain energies of the ring to be determined as functions of the generalized coordinates q_i $(i = 1 \ldots 4)$.

V. KINETIC ENERGY OF RING

If the effects of rotary inertia are neglected the kinetic energy of an elemental section of ring is determined by the absolute velocity $\mathbf{V}_P$ of its center of mass P. For an applied rate of turn $\boldsymbol{\Omega}$, $\mathbf{V}_P$ is given by

$$\mathbf{V}_P = \dot{\mathbf{r}} + \boldsymbol{\Omega} \times \mathbf{r} \tag{4}$$

and the kinetic energy of the ring follows as

$$T = \tfrac{1}{2}\rho A a \int_0^{2\pi} \mathbf{V}_P \cdot \mathbf{V}_P \, d\theta. \tag{5}$$

To evaluate this integral the rate of turn $\boldsymbol{\Omega}$ must be expressed in terms of components along the local polar coordinate directions at P. Thus

$$\begin{aligned} \Omega_r &= \Omega_x \cos\theta + \Omega_y \sin\theta \\ \Omega_\theta &= -\Omega_x \sin\theta + \Omega_y \cos\theta \\ \Omega_z &= \Omega_z. \end{aligned} \tag{6}$$

The substitution of (4) and (6) into (5) yields, after some rearrangement of terms, an expression for the kinetic energy as a function of the generalized coordinates

$$\begin{aligned} T = \tfrac{1}{2}\pi\rho a \int_0^{2\pi} \Bigg\{ & \dot{q}_1^2 \cos^2 n\theta + \dot{q}_2^2 \sin^2 n\theta + 2\dot{q}_1\dot{q}_2 \cos n\theta \sin n\theta \\ & + \frac{1}{n^2}(\dot{q}_1^2 \sin^2 n\theta + \dot{q}_2^2 \cos^2 n\theta - 2\dot{q}_1\dot{q}_2 \cos n\theta \sin n\theta) \\ & + \dot{q}_3^2 \cos^2 m\theta + \dot{q}_4^2 \sin^2 m\theta + 2\dot{q}_3\dot{q}_4 \cos m\theta \sin m\theta \\ & + \frac{2}{n}\Omega_z(q_1\dot{q}_2 - \dot{q}_1 q_2) \\ & + \Omega_x \Bigg[(q_1\dot{q}_4 - \dot{q}_1 q_4 + q_2\dot{q}_3 - \dot{q}_2 q_3)\sin(n+m)\theta \sin\theta \\ & \quad + (-q_1\dot{q}_4 + \dot{q}_1 q_4 + q_2\dot{q}_3 - \dot{q}_2 q_3)\sin(n-m)\theta \sin\theta \\ & \quad + (q_1\dot{q}_3 - \dot{q}_1 q_3 - q_2\dot{q}_4 + \dot{q}_2 q_4)\cos(n+m)\theta \sin\theta \\ & \quad + (q_1\dot{q}_3 - \dot{q}_1 q_3 + q_2\dot{q}_4 - \dot{q}_2 q_4)\cos(n-m)\theta \sin\theta \\ & \quad + \frac{1}{n}\{(q_1\dot{q}_4 - \dot{q}_1 q_4 + q_2\dot{q}_3 - \dot{q}_2 q_3)\cos(n+m)\theta \cos\theta \\ & \quad + (-q_1\dot{q}_4 + \dot{q}_1 q_4 + q_2\dot{q}_3 - \dot{q}_2 q_3)\cos(n-m)\theta \cos\theta \\ & \quad + (-q_1\dot{q}_3 + \dot{q}_1 q_3 - q_2\dot{q}_4 + \dot{q}_2 q_4)\sin(n-m)\theta \cos\theta \\ & \quad + (-q_1\dot{q}_3 + \dot{q}_1 q_3 + q_2\dot{q}_4 - \dot{q}_2 q_4)\sin(n+m)\theta \cos\theta\} \Bigg] \\ & + \Omega_y \Bigg[(-1)((q_1\dot{q}_4 - \dot{q}_1 q_4 + q_2\dot{q}_3 - \dot{q}_2 q_3)\sin(n+m)\theta \sin\theta \\ & \quad + (-q_1\dot{q}_4 + \dot{q}_1 q_4 + q_2\dot{q}_3 - \dot{q}_2 q_3)\sin(n-m)\theta \sin\theta \\ & \quad + (q_1\dot{q}_3 - \dot{q}_1 q_3 - q_2\dot{q}_4 + \dot{q}_2 q_4)\cos(n+m)\theta \sin\theta \\ & \quad + (q_1\dot{q}_3 - \dot{q}_1 q_3 + q_2\dot{q}_4 - \dot{q}_2 q_4)\cos(n-m)\theta \sin\theta) \\ & \quad + \frac{1}{n}\{(q_1\dot{q}_4 - \dot{q}_1 q_4 + q_2\dot{q}_3 - \dot{q}_2 q_3)\cos(n+m)\theta \cos\theta \\ & \quad + (-q_1\dot{q}_4 + \dot{q}_1 q_4 + q_2\dot{q}_3 - \dot{q}_2 q_3)\cos(n-m)\theta \cos\theta \\ & \quad + (-q_1\dot{q}_3 + \dot{q}_1 q_3 - q_2\dot{q}_4 + \dot{q}_2 q_4)\sin(n-m)\theta \cos\theta \\ & \quad + (-q_1\dot{q}_3 + \dot{q}_1 q_3 + q_2\dot{q}_4 - \dot{q}_2 q_4)\sin(n+m)\theta \cos\theta\} \Bigg] \Bigg\} d\theta. \end{aligned} \tag{7}$$

It can be seen, by inspection of (7), that the contribution made to the kinetic energy by the input rates Ω_x and Ω_y is only non-zero if the mode numbers (m,n) are chosen to satisfy the relationship $(m-n) = \pm 1$. For the purposes of describing the dynamics of the gyroscope the case $(m-n) = 1$ is investigated. When the integration over the interval $(0, 2\pi)$ is performed for (7), for the case $(m-n) = 1$, the kinetic energy can be written as

$$\begin{aligned} T = \frac{\pi}{2}\rho A a \Bigg\{ & \left(1 + \frac{1}{n^2}\right)(\dot{q}_1^2 + \dot{q}_2^2) + \dot{q}_3^2 + \dot{q}_4^2 + \frac{4\Omega_z}{n}(q_1\dot{q}_2 - \dot{q}_1 q_2) \\ & + \Omega_x \left(1 - \frac{1}{n}\right)(q_1\dot{q}_4 - \dot{q}_1 q_4 - q_2\dot{q}_3 + \dot{q}_2 q_3) \\ & + \Omega_y \left(1 - \frac{1}{n}\right)(-q_1\dot{q}_3 + \dot{q}_1 q_3 - q_2\dot{q}_4 + \dot{q}_2 q_4) \Bigg\}. \end{aligned} \tag{8}$$

A. Strain Energy of Ring

Strains in the ring arise due to bending and torsion and it follows that the strain energy V can be written as functions of the curvatures κ_1 and κ_2 and the torsion τ of the center line of the ring [5]. The strain energy of the ring can thus be written as

$$\begin{aligned} V_r = {} & \frac{EI_{zz}a}{2}\int_0^{2\pi} \kappa_1^2 \, d\theta + \frac{EI_{xx}a}{2}\int_0^{2\pi} \kappa_2^2 \, d\theta \\ & + \frac{GI_{\theta\theta}a}{2}\int_0^{2\pi} \tau^2 \, d\theta \end{aligned} \tag{9}$$

where the curvatures and torsion are given by

$$\kappa_1 = \frac{1}{a^2}\left(\frac{\partial^2 u}{\partial\theta^2} - \frac{\partial v}{\partial\theta}\right)$$
$$\kappa_2 = \frac{1}{a^2}\frac{\partial^2 w}{\partial\theta^2} - \frac{\beta}{a} \qquad \text{and} \tag{10}$$
$$\tau = \frac{1}{a}\frac{\partial\beta}{\partial\theta} + \frac{1}{a^2}\frac{\partial w}{\partial\theta}.$$

In the expressions for κ_2 and τ the quantity β represents the rotation of the section and can be represented in modal form as

$$\beta = \beta_3 \cos m\theta + \beta_4 \sin m\theta. \tag{11}$$

Thus substitution of (11) and (10) into (9) yields

$$V_r = \frac{EI_{zz}\pi}{2a^3}(1-n^2)(q_1^2+q_2^2) + \frac{EI_{xx}\pi}{2a^3} \times [(\beta_3 a + m^2 q_3)^2 + (\beta_3 a + m^2 q_4)^2] + \frac{GI_{\theta\theta}\pi}{2a^3}[(am\beta_3 + mq_3)^2 + (am\beta_4 + mq_4)^2]. \tag{12}$$

B. Strain Energy of Suspension

The precise form of the strain energy of the suspension will depend on the detailed design of the supporting ligaments and their spatial distribution around the ring. In this problem it is assumed that the ligaments are cyclically distributed around the ring in such a way that the nth in-plane and the mth out-of-plane modes each produce pairs of identical natural frequencies. There is no unique number of ligaments and for the important case $n = 2$ and $m = n + 1 = 3$ the results of [6] show that this degeneracy will occur if the ring is supported by any of 3, 5, 7, 8, 9, 11, 12…ligaments. For such an arrangement the strain energy of the ligament set must be of the form:

$$V_l = \tfrac{1}{2}k_n(q_1^2+q_2^2) + \frac{1}{2}\sum_{j=3}^{4}(k_{11}q_j^2 + 2k_{12}q_j\beta_j + k_{22}\beta_j^2) \tag{13}$$

where k_n and k_{ij} are the generalized stiffness coefficients of the ligament suspension.

VI. Equations of Motion

The equations of motion are derived using Lagrange's equation, with the Lagrangian $L = T - (V_r + V_l)$, and a Rayleigh dissipation function $D = c/2\sum_{j=1}^{4}\dot{q}_j^2$, to include the effects of damping. Since the effects of rotary inertia are neglected it follows that there is a proportional relationship between the twist coordinates β_3 and β_4 and the out-of-plane coordinates q_3 and q_4. This relationship is derived from $\partial(V_r + V_l)/\partial\beta_j = 0$, $j = 3$ and 4, and is given by

$$\frac{\beta_3}{q_3} = \frac{\beta_4}{q_4} = \mu = \frac{-m^2}{a}\left[\frac{1 + \dfrac{I_{\theta\theta}}{2I_{xx}(1+\nu)} + \dfrac{a^2}{\pi m^2}\dfrac{k_{12}}{EI_{xx}}}{1 + \dfrac{m^2 I_{\theta\theta}}{2I_{xx}(1+\nu)} + \dfrac{a}{\pi}\dfrac{k_{22}}{EI_{xx}}}\right]. \tag{14}$$

The substitution of this relationship into L and the application of Lagrange's equation

$$\frac{d}{dt}\left(\frac{\partial L}{\partial\dot{q}_j}\right) - \frac{\partial L}{\partial q_j} + \frac{\partial D}{\partial\dot{q}_j} = 0,$$

yields the equation of motion of the gyroscope, which may be written, for the case $m = n + 1$ as

$$\ddot{\mathbf{q}} + 2\begin{bmatrix} 0 & -\lambda\Omega_z & \lambda''\Omega_y & -\lambda''\Omega_x \\ \lambda\Omega_z & 0 & \lambda''\Omega_x & \lambda''\Omega_y \\ -\lambda'\Omega_y & -\lambda'\Omega_x & 0 & 0 \\ \lambda'\Omega_x & -\lambda'\Omega_x & 0 & 0 \end{bmatrix}\dot{\mathbf{q}} + \begin{bmatrix} 2\xi_1\omega_1 & 0 & 0 & 0 \\ 0 & 2\xi_1\omega_1 & 0 & 0 \\ 0 & 0 & 2\xi_2\omega_2 & 0 \\ 0 & 0 & 0 & 2\xi_2\omega_2 \end{bmatrix}\dot{\mathbf{q}} + \begin{bmatrix} \omega_1^2 & 0 & 0 & 0 \\ 0 & \omega_1^2 & 0 & 0 \\ 0 & 0 & \omega_2^2 & 0 \\ 0 & 0 & 0 & \omega_2^2 \end{bmatrix}\mathbf{q} = \mathbf{0}. \tag{15}$$

In the absence of rates of turn, (15) shows that the modes are uncoupled and that the in-plane modes (q_1, q_2) and the out-of-plane modes (q_3, q_4) are characterized by undamped natural frequencies

$$\omega_1 = \sqrt{\frac{EI_{zz}(1-n^2)^2}{A\rho a^4\left(1+\dfrac{1}{n^2}\right)} + \frac{k_n}{A\rho a\pi\left(1+\dfrac{1}{n^2}\right)}} \qquad \text{and} \tag{16}$$

$$\omega_2 = \sqrt{\frac{1}{\pi\rho A a}\left\{\frac{E\pi}{a^3}\left[I_{xx}(\mu a + m^2)^2 + \frac{I_{\theta\theta}}{2(1+\nu)}(\mu a m + m)^2\right] + k_{11} + 2\mu k_{12} + \mu^2 k_{22}\right\}}.$$

If the effect of the ligaments is ignored these reduce to the well-known expression [5]

$$\omega_1 = \sqrt{\frac{EI_{zz}(1-n^2)^2}{A\rho a^4\left(1+\dfrac{1}{n^2}\right)}} \qquad \text{and}$$
$$\omega_2 = \sqrt{\frac{EI_{xx}(m^2-1)^2}{\rho A a^4}\left[1 + \frac{2(1+\nu)I_{xx}}{m^2 I_{\theta\theta}}\right]^{-1}}. \tag{17}$$

When a rate of turn is applied it can be seen that the in-plane modes are gyroscopically coupled to each other and the out-of-plane modes and that there is no gyroscopic coupling between the out-of-plane modes. The factors

$$\lambda = \frac{2n}{n^2+1} \qquad \lambda' = \frac{n-1}{2n} \qquad \lambda'' = \frac{n(n-1)}{2(n^2+1)} \tag{18}$$

are the gyroscopic coupling factors and determine the degree of modal interaction in the presence of a general rate of turn.

VII. OPERATION AS GYROSCOPE

When the structure is operated as a rate gyro the primary mode q_1 is driven into self-oscillation at its natural frequency with its amplitude maintained at a set value by means of an amplitude control loop [3]. For these circumstances the motion of primary mode becomes independent of any rate of turn and the modal coordinate is given by

$$q_1 = q_{01} \sin \omega_1 t. \tag{19}$$

It now follows from (15) that the responses of the secondary motions to rates of turn are given by

$$\begin{aligned} \ddot{q}_2 + 2\xi_1\omega_1\dot{q}_2 + \omega_1^2 q_2 &= -2\lambda\Omega_z\omega_1 q_{01}\cos\omega_1 t \\ \ddot{q}_3 + 2\xi_2\omega_2\dot{q}_3 + \omega_2^2 q_3 &= 2\lambda'\Omega_y\omega_1 q_{01}\cos\omega_1 t \\ \ddot{q}_4 + 2\xi_2\omega_2\dot{q}_2 + \omega_2^2 q_2 &= -2\lambda'\Omega_x\omega_1 q_{01}\cos\omega_1 t. \end{aligned} \tag{20}$$

It is noticed that the cross coupling terms between the secondary motions due to rates of turn have been neglected. Such terms produce small contributions of $O((\Omega_\alpha/\omega_1)^2 q_{01})$, to the final response and are thus neglected. The solution to (20) gives the secondary motions as

$$\begin{aligned} q_2 &= -\frac{\lambda\Omega_Z}{\xi_1\omega_1} q_{01}\cos\omega_1 t \\ q_3 &= \frac{2\lambda'\Omega_y\omega_1}{\sqrt{(\omega_2^2-\omega_1^2)^2 + 4\xi_2^2\omega_1^2\omega_2^2}} q_{01}\cos(\omega_1 t - \varphi) \\ q_4 &= -\frac{2\lambda'\Omega_x\omega_1}{\sqrt{(\omega_2^2-\omega_1^2)^2 + 4\xi_2^2\omega_1^2\omega_2^2}} q_{01}\cos(\omega_1 t - \varphi) \end{aligned} \tag{21}$$

where

$$\varphi = \tan^{-1}\left(\frac{2\xi_2\omega_1\omega_2}{\omega_2^2-\omega_1^2}\right). \tag{22}$$

It follows from (21) that outputs generated from measurements of the respective secondary motions will provide a means of determining the components of the applied rate of turn. An applied rate about OZ produces a "tuned" response in the secondary motion q_2 and the amplitude of the motion is determined by the bandwidth $B = 2\xi_1\omega_1$, of the in-plane motion. In this respect the device responds in a manner that is identical to the single axis ring gyroscopes described in [1, 10, 11].

The responses generated by rates about OX and OY is determined by the degree of miss tuning between the natural frequencies of the in-plane and out-of-plane modes. For this case the performance of the ring is similar to those gyroscopes described in [17]. This reduced sensitivity to applied rate places an increased demand on the sensitivity of the "pick off" system used to measure the out-of-plane response. It is also seen that the factor

$$\frac{\lambda'}{\lambda} = \frac{(n-1)(n^2+1)}{4n^2}$$

is less than unity for the important case of $n = 2$. In this case the rate of turn about OZ has a greater gyroscopic coupling into its corresponding secondary mode.

A. Tuning

For this case suppose that the out-of-plane natural frequency can be written as $\omega_2 = \omega_1(1+\eta)$, where $\eta \ll 1$ is a miss-tuning factor. If first-order terms are retained the modal response q_4 becomes

$$q_4 = -\frac{\lambda'\Omega_x}{\xi_2\omega_1}\frac{1}{\sqrt{\left(1+\frac{\eta^2}{\xi_2^2}\right)}} q_{01}\cos(\omega_1 t - \varphi) \tag{23}$$

and

$$\varphi = \tan^{-1}\left(\frac{\xi_2}{\eta}\right). \tag{24}$$

To achieve a response of the same order as the secondary mode q_2 it is necessary to make $0 \le \eta \le \xi_2$.

B. Structure Geometry for Modal Tuning

To achieve tuning between the in-plane and out-of-plane modes one option is to match the in-plane width of the ring b to the out-of-plane thickness d of the structure. This can only be achieved once the ligament configuration has been defined. If, for example, the stiffness effects of the ligaments are ignored then equating the expressions for ω_1 and ω_2 given by (17) will yield a width-to-depth ratio $b/d = 2.854$. To illustrate the effect of the supporting suspension consider the example of a ring of radius 4 mm, width 285.4 μm and thickness 100 μm supported by a set of 8 ligaments. The ligaments are chosen to be uniformly distributed around the

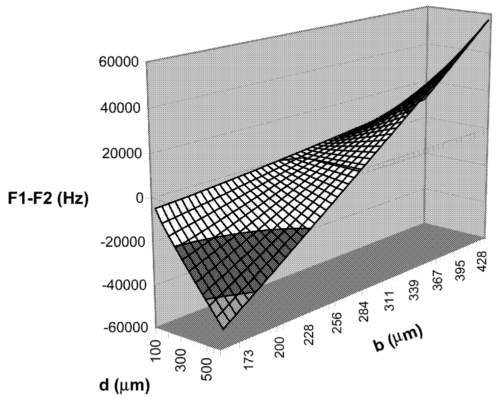

Fig. 5. Frequency split versus ring width and thickness.

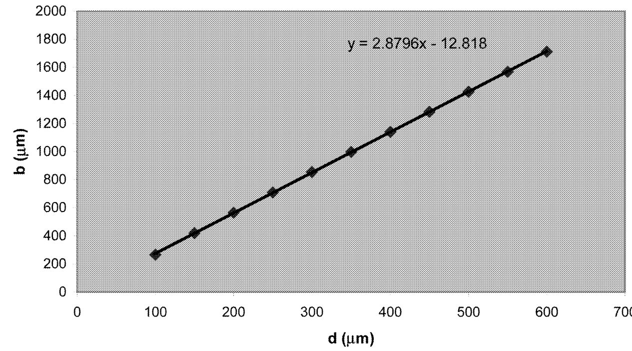

Fig. 6. Equation of line of intersection with plane $F_1 - F_2 = 0$.

circumference of the ring and adjacent ligaments are separated by angle of $\pi/4$. In this case the ring width and thickness values were chosen such that if the ligaments are ignored, the in-plane and out-of-plane modes of vibration are tuned. The form of each ligament is shown in Figs. 7 and 9 with dimensions $L_1 = 250\ \mu$m, $L_2 = 1000\ \mu$m, and $L_3 = 250\ \mu$m. It is assumed that each ligament has a width $h = 20\ \mu$m and a thickness the same as that of the ring. For this configuration the application of the theory outlined in Appendix B yields generalized stiffness values:

$k_n = 2 \times 10^3$ Nm^{-1}
$k_{11} = 125$ Nm^{-1}
$k_{12} = 1.3 \times 10^{-2}$ N
$k_{22} = 6.7 \times 10^{-5}$ Nm

For these dimensions the natural frequencies of the supported and unsupported rings can be calculated from (16) and (17) and have the values (f_1 = 20.51 KHz, f_2 = 19.39 KHz) and (f_1 = 19.29 KHz, f_2 = 19.29 KHz), respectively. For this case it is seen that the suspension has greatest effect on the frequencies of the in-plane motion. Finite element analysis of the supported ring was employed to compare with the analytical model. Finite element analysis yields frequencies with values f_1 = 19.43 KHz and f_2 = 17.84 KHz which are less than the analytically derived values of (16) by 5.6% and 8.7%, respectively. The difference is partially accounted for by noting that the analytical model will overestimate the frequencies because the inertial effects of the ligaments are neglected.

By selecting different values for the ring thickness and width the frequency split $(f_1 - f_2)$ can be plotted as the surface, shown in Fig. 5. It is clear from Fig. 5 that there exists a particular relationship between the width and thickness of the ring that will result in tuning between the in-plane and out-of-plane modes of vibration. The equation of the line that intersects the plane $(f_1 - f_2) = 0$ can be found by fixing the thickness d and finding the corresponding value of the width b which result in a frequency split of zero. This line is illustrated in Fig. 6. For this range of values the relationship between width b and thickness d is approximately linear and has the form $b = 2.88d - 13$ where b and d are both expressed in micrometers. If the ring width b is held fixed at 285.4 μm the thickness for tuning becomes $d = 103.6\ \mu$m and the corresponding frequencies are $f_1 = f_2 = 20.51$ KHz. Only the natural frequency of the out-of-plane motion is changed and it is an increase in the thickness of the structure producing a more than proportional increase in flexural stiffness that causes the natural frequency of the out of plane motion to be increased.

C. Fine Tuning by Electrostatic Actuation

Because of manufacturing imperfections it is unlikely that the ring can be manufactured to the precise dimensions required for perfect tuning of the in-plane and out-of-plane modes. To overcome this problem it is proposed that the dimensions of the structure be chosen to produce a small positive miss-tuning, $\Delta f = f_2 - f_1 \succ 0$, and to then tune by reducing the out-of-plane flexural stiffness of the ring using electrostatic actuation similar to that proposed in [11]. In this case the ring will be held at Earth potential and a continuous annular electrode, held at a steady potential V, will be located a distance z_0 directly above the ring, as shown in Fig. 1. An analysis of the generalized force produced by this electrode, due to the out-of-plane motion w, (see Appendix C), shows that small amounts of miss-tuning can be offset by setting

$$\Delta f = \frac{\varepsilon_0 V^2}{8\pi^2 \rho z_0^3 d f_1} \tag{25}$$

For example, if a miss-tuning of the order of 200 Hz is designed for, then, for the ring dimensions assumed in Sec. VIIB and for $z_0 = 1\ \mu$m, (25) gives a value for applied voltage of the order $V \sim 3$ V. These values suggest that fine-tuning of the modes is feasible.

VIII. CONCLUSION

A structure based upon a supported ring has been investigated for application as a three-axis rate of turn sensor. An in-plane mode of the ring (of order n) is used to provide the primary motion of the gyroscope and an in-plane mode (order n) and two out-of-plane modes (order m) provide the secondary response to rates of turn. To provide modal degeneracy in these modes of vibration the need to have a cyclic-symmetric suspension, formed from an array of ligaments, has been discussed. The equation of motion for the gyroscope for the important case where the mode numbers satisfy $m = n + 1$ have been derived and it has been shown that the rate measurement is proportional to the corresponding gyroscopic coupling factor. The responses to constant rates of turn have been evaluated. For the $n = 2$ case, the response to a rate of rotation about OZ has been shown to be a factor 16/5 greater than the response to rates about OX and OY. The miss-tuning η between the in-plane and out of plane modes is shown to be important and kept below the value of the secondary mode damping factor ξ_2. For this case the secondary response to rates of turn about OX and OY will be of the same order as the response to rates of turn applied about OZ. One way of minimizing the miss-tuning factor is to adjust the ring width to thickness ratio b/d, to a value that results in tuning between the in-plane and out-of-plane modes. If the effect of the support ligaments is ignored this ratio has a value of $b/d = 2.854$. It is shown how this ratio must be adjusted if the effect of the support ligaments cannot be ignored. A procedure of fine-tuning using electrostatic actuation is shown to be feasible.

APPENDIX A. TORSIONAL RIGIDITY OF RECTANGULAR SHAFT

The torsional rigidity of a shaft of rectangular cross section is given by $GI_{\theta\theta}$ where $I_{\theta\theta}$ is the torsional section factor and

$$G = \frac{E}{2(1+v)}.$$

An expression for $I_{\theta\theta}$ for a cross section of width b and thickness h is given by [4],

$$I_{\theta\theta} = \frac{hb^3}{3}\left[1 - \frac{192}{\pi^5}\frac{b}{h}\sum_{i=1}^{\infty}\frac{1}{(2i-1)^5}\tan h\frac{(2i-1)\pi h}{2b}\right]. \tag{26}$$

APPENDIX B. GENERALIZED STIFFNESS OF SUPPORTING LIGAMENTS

To illustrate the procedure used to estimate the generalized stiffness of the supporting ligaments we assume a particular ligament form. The form assumed

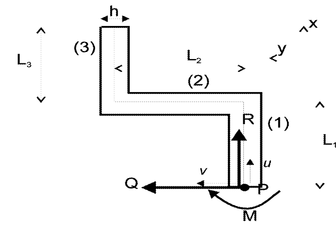

Fig. 7. Applied moments due to in-plane vibration of ring.

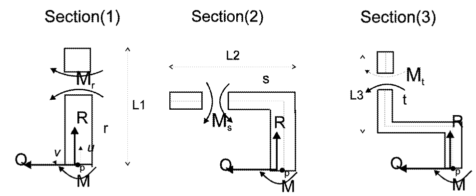

Fig. 8. Bending moments due to in-plane vibration of ring.

is shown in Figs. 7 and 9. In this case the ligament is composed of three straight beams, of constant rectangular cross section, which are connected so that the center lines of adjacent beams are set perpendicular to each other. Point P on the ligament is constrained to have the same displacements as the corresponding point on the ring and it is assumed that the "far end" is fully fixed to the supporting substrate. The estimate of the generalized stiffness is based on an energy method and takes advantage of Castigliano's Theorem.

In-plane Motion: Suppose that the point of connection P has radial and tangential displacements u_P and v_P and that the rotation of the ring's center line at P is

$$\phi_P = \frac{1}{a}\left(\frac{\partial u}{\partial \theta} - v\right).$$

Because of these displacements the ring applies radial and tangential forces R and Q and a moment M to the ligament, as shown in Fig. 7. The bending moments M_r, M_s, and M_t at different sections in the ligament are shown in Fig. 8 and these are given by

$$M_r = M + Qr$$
$$M_s = M + QL_1 - Rs$$
$$M_t = M + Q(L_1 + t) - RL_2.$$

The strain energy in the ligament can now be expressed in terms of these bending moments and is given by

$$V = \frac{1}{2EI'_{zz}}\left(\int_0^{L_1} M_r^2\,dr + \int_0^{L_2} M_s^2\,ds + \int_0^{L_3} M_t^2\,dt\right) \tag{27}$$

where $I'_{zz} = \frac{1}{12}dh^3$.

It now follows from Castigliano's Theorem that the displacements at P are given by

$$u_P = \frac{\partial V}{\partial R}, \qquad v_P = \frac{\partial V}{\partial Q} \qquad \text{and} \qquad \phi_P = \frac{\partial V}{\partial M}.$$

An evaluation of these relationships shows that they may be expressed in the matrix form

$$\begin{bmatrix} u_P \\ v_P \\ \phi_P \end{bmatrix} = H \begin{bmatrix} R \\ Q \\ M \end{bmatrix} \tag{28}$$

where H is the called the flexibility matrix of the ligament at P. The stiffness matrix of the ligament at P is thus

$$K = H^{-1}. \tag{29}$$

To obtain the generalized stiffness matrix of the suspension the displacement at P is first rewritten as

$$\begin{bmatrix} u_P \\ v_P \\ \phi_P \end{bmatrix} = \begin{bmatrix} \cos n\theta_P \\ -\dfrac{1}{n}\sin n\theta_P \\ \dfrac{1}{a}\dfrac{(1-n^2)}{n}\sin n\theta_P \end{bmatrix} q_1 = A_P q_1. \tag{30}$$

The strain energy of the suspension can now be written as a function of the generalized coordinate and is

$$V = \frac{1}{2}\left(\sum_P A_P^T K A_P\right) q_1^2. \tag{31}$$

The generalized stiffness of the suspension shown in Fig. 1, for the case $n = 2$, thus follows as

$$k_n = \sum_{P=1}^{8} A_P^T K A_P = 4\left(K_{11} + \frac{1}{2}K_{22} + \frac{9}{4a^2}K_{33}\right) \tag{32}$$

and is only a function of the direct stiffnesses of the ligament. Since (1) and (2) represent approximations to the true mode shapes of the supported structure it is reassuring to find that if the above exercise is repeated for a displaced shape corresponding to the secondary mode the same expression for k_n is found.

Out-of-Plane Motion: The procedure used to estimate the generalized stiffness of the suspension for the out-of-plane motion follows along similar lines to that given above. In this case the displacements and rotations at P are given by

$$\begin{bmatrix} w_P \\ \beta_P \\ \varphi_P \end{bmatrix} = \begin{bmatrix} w_P \\ \beta_P \\ \left(\dfrac{1}{a}\dfrac{\partial w}{\partial \theta}\right)_P \end{bmatrix} = \begin{bmatrix} \cos m\theta_P & 0 \\ 0 & \cos m\theta_P \\ -\dfrac{m}{a}\sin m\theta_P & 0 \end{bmatrix} \begin{bmatrix} q_3 \\ \beta_3 \end{bmatrix}$$

$$= B_P \begin{bmatrix} q_3 \\ \beta_3 \end{bmatrix}. \tag{33}$$

These displacements produce reactions (W, M_d, M_g), Fig. 9, on the ligament at P and in turn these generate bending and twisting moments on the different

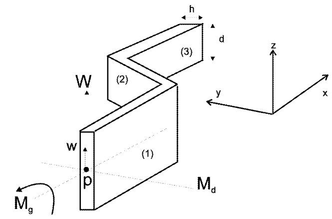

Fig. 9. Applied moments due to out-of-plane vibration of ring.

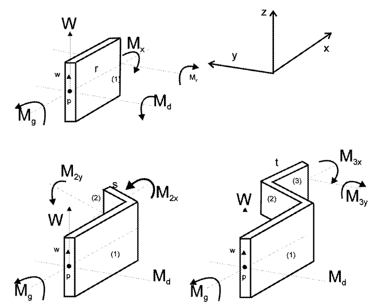

Fig. 10. Bending and twisting moments due to out-of-plane vibration of ring.

sections of the ligament as shown in Fig. 10. The strain energy in each beam section of the ligament is thus

$$\begin{aligned}
V_1 &= \frac{1}{2GI'_{\theta\theta}}\int_0^{L_1} M_g^2\,dr + \frac{1}{2EI'_y}\int_0^{L_1}(M_d - Wx)^2\,dr \\
V_2 &= \frac{1}{2GI'_{\theta\theta}}\int_0^{L_2}(M_d - L_1 W)^2\,ds \\
&\quad + \frac{1}{2EI'_y}\int_0^{L_2}(M_t + Ws)^2\,ds \\
V_3 &= \frac{1}{2GI'_{\theta\theta}}\int_0^{L_3}(M_t + L_2 W)^2\,dt \\
&\quad + \frac{1}{2EI'_y}\int_0^{L_3}(M_d - V(L_1 + t))^2\,dt
\end{aligned} \tag{34}$$

and $V = V_1 + V_2 + V_3$. In these equations $I'_y = hd^3/12$ and $I'_{\theta\theta}$ is the torsional section factor defined in Appendix A. The stiffness matrix S at P now follows from an analysis of $w_P = \partial V/\partial W$, $\beta_P = \partial V/\partial M_d$, and $\varphi_P = \partial V/\partial M_g$ (in a manner similar to that shown by (30) and (33)) and it follows that the generalized stiffness matrix of the suspension is given by

$$k = \begin{bmatrix} k_{11} & k_{12} \\ k_{12} & k_{22} \end{bmatrix} = \sum_P B_P^T S B_P.$$

For the case of $P = 12$ and $m = 3$ the generalized stiffness matrix has the value

$$k = 4\begin{bmatrix} S_{11} + \dfrac{9}{a^2}S_{33} & S_{12} \\ S_{12} & S_{22} \end{bmatrix}.$$

APPENDIX C. ELECTROSTATIC ADJUSTMENT

Fig. 1 shows a capacitor formed by the ring, assumed to held at zero potential and a fixed electrode positioned a nominal distance z_0 above the ring. If this electrode is held at a voltage V and if the ring is displaced vertically an amount $w = q_3 \cos m\theta$ the energy stored in the capacitor can be written

$$V_C = \frac{\varepsilon_0 abV^2}{2z_0}\int_0^{2\pi}\left(1+\frac{q_3}{z_0}\cos m\theta + \left(\frac{q_3}{z_0}\right)^2\cos^2 m\theta + \cdots\right)d\theta. \tag{35}$$

The generalized force associated with the capacitor follows, to a first order in (q_3/z_0), as

$$F_c = \frac{\partial V_c}{\partial q_3} = \frac{\varepsilon_0 \pi abV^2}{z_0^3}q_3. \tag{36}$$

If this force is now divided by the generalized mass of the mode, $\pi\rho abd$, it follows that the natural frequency of the out-of-plane mode is reduced and becomes determined from

$$\omega_{2\,\mathrm{Elec}}^2 = \omega_2^2 - \frac{\varepsilon_0 V^2}{\rho d z_0^3}. \tag{37}$$

REFERENCES

[1] Burdess, J. S. (1986)
The dynamics of a thin piezoelectric cylinder gyroscope.
Proceedings of the Institution of Mechanical Engineers, **200**, C4 (1986), 271–280.

[2] Burdess, J. S., and Wren, T. (1986)
The theory of a piezoelectric disc gyroscope.
IEEE Transactions on Aerospace and Electronic Systems, **AES-22**, 4 (July 1986).

[3] Burdess, J. S. (1997)
UK Patent GB-B-2154739, 1997.

[4] Timoshenko, S. P., and Goodier, J. N. (1970)
Theory of Elasticity.
New York: McGraw-Hill, 1970.

[5] Love, A. E. H. (1927)
A treatise on the mathematical theory of elasticity.
London: Cambridge University Press, 1927.

[6] Thomas, D. L. (1979)
Dynamics of rotationally periodic structures.
International Journal for Numerical Methods in Engineering, **14** (1979), 81–102.

[7] Benham, P. P. (1987)
Mechanics of Engineering Materials.
New York: Wiley, 1987.

[8] Bryan, G. H. (1890)
On a revolving cylinder or bell.
Proceedings of the Royal Society (London), **47** (1890).

[9] Timoshenko, S. P. (1937)
Vibration Problems in Engineering.
London: Constable, 1937.

[10] Harris, A. J., Burdess J. S., Wood, D., Langford, R., Williams, G., Ward, M. C. L., and McNie, M. E. (1998)
Issues associated with the design, fabrication and testing of a crystalline silicon ring gyroscope with electromagnetic actuation and sensing.
Journal of Micromechanical Microengineering, **8** (1998), 284–292.

[11] Putty, M. W., and Najafi, K. (1994)
A micromachined vibrating ring gyroscope.
In *Proceedings of the Solid State Sensor and Actuator Workshop*, Hilton Head, SC, 1994, 213–220.

[12] Langhaar, H. L. (1962)
Energy Methods in Applied Mechanics.
New York: Wiley, 1962.

[13] Fell, C. P. (1999)
US Patent 5,915,276, 1999.

[14] Geiger, W., Kieninger, M., Pascal, M., Folkmer, B., and Lang, W. (1998)
Micromachined angular rate sensor MARS-RR.
In *Proceedings of the SPIE Conference on Micromachined Devices and Components IV*, **3514** (1998).

[15] Loper, E., and Lych, D. D. (1982)
The HRG: A new low noise inertial rate sensor.
In *Proceedings of the 16th JT Services Data Exchange for Inertial Systems*, Los Angeles, CA, 1982, 16–18.

[16] Hopkin, I. D. (1997)
The performance and design of a silicon micromachined gyro.
Presented at the Symposium Gyro Technology 1997, Stuggart, Germany.

[17] Yazdi, N., Ayazi, F., and Najafi, K. (1998)
Micromachined inertial sensors.
Proceedings of the IEEE, **86**, 8 (Aug. 1998).

[18] Juneau, T., Pisano, A. P., and Smith, J. H. (1997)
Dual axis operation of a micromachined rate gyroscope.
In *Technical Digest of the 9th International Conference on Solid State Sensor & Actuator (Tranducers 97)*, Chicago, IL, June 1997, 883–886.

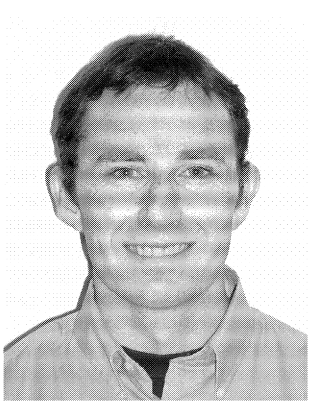

Barry J. Gallacher completed his B.Sc. in physics from the University of Glasgow, UK in 1994 with an honours degree in physics.

After graduation he was employed as an engineer within the microelectronics industry first with GEC Plessey Semiconductors and then with Siemens Microelectronics. He currently holds the post of Research Associate within the Department of Mechanical, Materials and Manufacturing Engineering, Newcastle University, where he is currently working towards his Ph.D. degree in micromechanics.

James S. Burdess graduated from the University of Newcastle upon Tyne, UK in 1968 with a first class honours degree in mechanical engineering.

After graduation he carried out research in vibration theory and was awarded the Ph.D. degree in 1973 for work on transmission systems driven by variable velocity couplings. He is currently a Professor in Engineering Dynamics at Newcastle University and has research interests in the fields of gyrodynamics, active vibration control and power transmissions systems.

Prof. Burdess is a Chartered Engineer and a Member of the Institution of Mechanical Engineers.

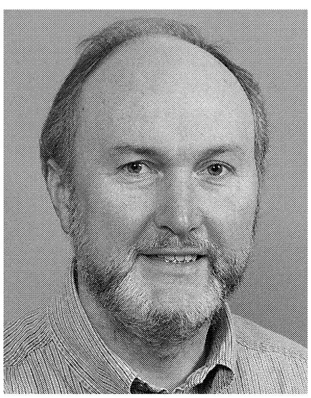

Alun James Harris is a lecturer in the Department of Electrical & Electronic Engineering at the University of Newcastle, UK. His research interests include micromechanics, optoelectronics, sensors and actuators. In the field of micromechanics, current research includes the development of optical testing and processing methods and the study of vibratory structures with particular application to microgyros. In collaboration with other members of the Centre for Nanoscale Science and Technology MEMS sensors are being developed for medical and biological applications.

Mark E. McNie completed his B.Sc. in physics from Imperial College in 1990 and his M.Sc. in electronics from the University of Nottingham in 1991.

He worked on HBT technology before joining QinetiQ (formerly DERA) in 1995 to work on silicon-based MEMS process technologies and devices. His research interests include microinertial and optical MEMS devices.

Mr. McNie is currently a chapter chairman on SEMI International "Commercialisation of MEMS" roadmap, a member of the IEE, and has published many papers in the field.